# Generation of 5.2 fs, energy scalable blue pulses

Feilong Hu,[1] Qingbin Zhang,[1,*] Jinxing Cao,[1] Zuofei Hong,[2,4] Wei Cao,[1,5] and Peixiang Lu[1,2,3,6]

[1]*School of Physics and Wuhan National Laboratory for Optoelectronics, Huazhong University of Science and Technology, Wuhan 430074, China*
[2]*Hubei Key Laboratory of Optical Information and Pattern Recognition, Wuhan Institute of Technology, Wuhan 430205, China*
[3]*Optics Valley Laboratory, Hubei 430074, China*
[4]*e-mail: zuofei.hong@wit.edu.cn*
[5]*e-mail: weicao@hust.edu.cn*
[6]*e-mail: lupeixiang@hust.edu.cn*
*Corresponding author: zhangqingbin@hust.edu.cn*

**In this Letter, ultrashort blue pulses spanning 350–500 nm are generated by combining the broadband frequency doubling technology with the two-stage multiplate continuum (MPC) generation scheme. We prepare relatively broadband input pulses and use a two-stage configuration for MPC generation, allowing us to employ thinner and less solid plates for further spectral broadening. Therefore, the deteriorations of the spectral phase, energy conversion efficiency, and beam quality, which occur more easily for 400 nm pulses, are effectively suppressed. After fine dispersion management, we obtain clean 5.2 fs blue pulses with a root-mean-square energy stability of 0.69% over one hour and excellent beam quality. Furthermore, lower than 8% energy loss during the spectral broadening process at each stage is achieved. The overall optimized performances and energy scalability of this blue pulse, as well as the possibility of further compressing the pulse duration, are likely to motivate more strong-field research with sub-cycle time resolution in this extended wavelength range.** © 2022 Optica Publishing Group

With the capacity of controlling a waveform, few-cycle laser pulses have succeeded in opening the door to attosecond science [1] and laser-triggered petahertz electronics [2]. To further develop applications of few-cycle pulses, one crucial issue is to extend the central wavelength into a shorter region. Compared with the commonly used 800 nm laser, a 400 nm laser with shorter wavelength and higher photon energy has shown many unique facilitations in ultrafast and strong-field studies.

In recent strong-field ionization studies, it has been theoretically predicted that for the generation of distinguishable electron vortex under the multiphoton ionization regime, the target atoms can be extended from the alkali atom K [3] to the more generally used noble gas atom Xe [4] with few-cycle 400 nm pulses. Owing to the high-order harmonic (HH) yield scales of approximately $\lambda^{-6}$ [5,6], where $\lambda$ is the center wavelength of the driving laser, the reported HH yield for a 400 nm laser is approximately 60 times higher than that for a 800 nm laser [6]. If one can compress the 400 nm pulses down to 6.5 fs, it is also very attractive for

efficiently producing isolated attosecond pulses using the generalized double optical gating (GDOG) technology [7]. Thus, few-cycle 400 nm pulses with much lower energy can be used to drive the attosecond NUV (near ultraviolet)–XUV (extreme ultraviolet) pump-probe spectroscopy experiment, which is quite suitable for one-photon excited ultrafast charge-carrier dynamic research of wide-bandgap semiconductors [8]. The 400 nm few-cycle pulses also can be used for time-resolved spectroscopy experiments to detect the ultrafast vibration processes of samples, which have strong absorption in the NUV [9]. In addition, it is possible for sub-cycle dynamic research and control of electron pulses for the generation of carbon nanotubes [10] with few-cycle 400 nm pulses. Therefore, it is worthwhile to develop proper schemes for few-cycle 400 nm pulse generation.

One typical route for few-cycle 400 nm pulse generation is direct frequency up-conversion of broadband long-wavelength pulses, including second harmonic generation (SHG) [11], sum-frequency generation (SFG) [12], broadband frequency doubling [13], achromatic frequency doubling [14,15], and so on. Generally, sub-10 fs, 400 nm pulses can be obtained with an energy range from few μJ [12] to hundreds of μJ level [11,13] using this route. However the sub-10 fs pulse duration is not short enough. For achromatic frequency doubling, the phase-matching bandwidth can be significantly improved with high conversion efficiency and eliminated high-order angular dispersion. Therefore, the 7 fs UV pulses in [14] and 380–530 nm second harmonic spectrum in [15] have been achieved. Nevertheless, the obtained pulse energy after compression is still in the sub-μJ level at present, which prevents this scheme from the strong-field applications.

Another is through hollow-core fiber (HCF)-based postcompression or dispersion wave emission (DWE). For typical post-compression of the broadened 400 nm supercontinuum with chirped mirrors (CMs) [9,16], the obtained pulse duration is between 8 and 10 fs, owing to the easily accumulated high-order dispersion in the spectral broadening process and mediums (such as glass windows). In addition, the maximal 6 μJ, 4.4 fs, 400 nm pulses have been achieved by post-compressing (with CMs) the 350–500 nm spectrum, which is spectrally split from the 800 μJ octave-spanning supercontinuum output from an HCF

[8]. However, its energy scalability is limited owing to the weak energy near the short-wave end of the supercontinuum. DWE in an HCF has been demonstrated as a promising way to generate 3 fs NUV pulses with 20 μJ energy [17,18]. However, there are some non-negligible challenges in spectrally splitting the DWE thoroughly from a ultra-broadband supercontinuum (300–2500 nm) for performing experiments without the disturbances of the other frequency components.

In recent years, with flexible, robust and low-cost characteristics, the multiplate continuum (MPC) generation scheme has achieved great development in few-cycle pulse generation [19–22]. Especially, it has exhibited obvious advantages in compressing broadband short pulses into a shorter few-cycle [23] and even single-cycle [21] region. Nevertheless, there are more challenges in compressing 400 nm pulses [20,24]. On the one hand, the broadened spectrum is not broadband enough at present, only supporting a 7 fs Fourier-transform limit (FTL) pulse duration. On the other hand, the easily occurring beam quality degradation caused by multifilamentation formation and higher ionization rate during the spectral broadening process obstruct its applications.

Here, we demonstrate the generation of 7.8 μJ, 5.2 fs blue pulses by combining the relatively broadband and short 400 nm input pulse generation with two-stage MPC generation. We use thinner and fewer plates to avoid the occurrences of multifilamentation formation, excessive ionization, and high-order dispersion accumulation. The obtained supercontinuum can still span the 350–500 nm region with short input pulses and two-stage spectral broadening. By finely controlling the dispersion during the whole pulse compression process, 5.2 fs clean pulse compression is achieved. At the same time, the energy loss during spectral broadening process is effectively decreased. Furthermore, the excellent beam quality and high power stability of the output pulses [0.69% root mean square (rms) over 1 hour] are maintained.

The schematic of the experimental set-up is shown in Fig. 1. The 409 μJ pulses are directly output from a 1 m long, 250 μm inner diameter HCF. Its spectrum is broadened slightly and can support 16.4 fs FTL pulse duration. By introducing positive chirp into the input pulses, we can obtain the M-shape spectrum, as shown in Fig. 2(a), which stems from the
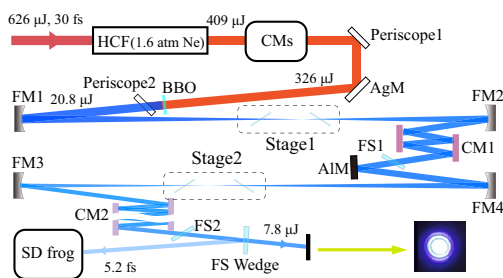
self-phase modulation (SPM) process in the HCF [11]. After dispersion compensation with CMs, the 800 nm pulses are compressed to 17.6 fs, as shown in Fig. 2(b), which is diagnosed by our home-built self-diffraction frequency-resolved optical gating (SD-FROG) [8,9]. Subsequently, the 326 μJ s-polarization fundamental wavelength (FW) pulses are input into a 100 μm thick beta barium borate (BBO) crystal with a cutting angle of 29.2° for SHG.

By optimizing the BBO angle, maximal 20.8 μJ SHG pulses are measured, with a spectrum spanning approximately 50 nm, as shown in Fig. 2(a). The spectrum can support a 15.4 fs FTL pulse duration, which is even shorter than the FTL pulse duration of FW pulses. The effective improvement of bandwidth of SHG pulses is attributed to the M-shape FW spectrum weakens the gain narrowing effect in the SHG process [11]. Even though the residual high-order dispersion and the excessive spectral modulation depth of FW pulses result in the existence of two obvious satellite pulses beside the main pulse, a much better temporal structure of 400 nm pulses without noticeable shoulder, as shown in Figs. 2(c), 2(d), can still be achieved owing to the SHG being a sensitive intensity-dependent process. The retrieved pulse duration is 22.8 fs with a reconstruction error of 0.0032. If we artificially remove the dispersion of 1.7 m long air and neglect the dispersion introduced by the dielectric films of the dichroic mirror simultaneously, the estimated pulse duration at the position of the BBO is 16.1 fs, very close to the FTL pulse duration. The generation of much shorter and more broadband SHG pulses than previous work [9,20] with admirable phase characteristic provides the critical preconditions for achieving wider spectral broadening and easier dispersion compensation in the subsequent MPC. It is worth mentioning that owing to the imperfect pulse compression, the relative low intensity of FW pulses and reflective loss of Periscope2, a conversion efficiency of only 6.4% is achieved. However, we believe that there is much room for improvement of the SHG efficiency with better pulse compression and higher laser intensity.

The SHG beam is focused by FM1. The focused beam waist diameter is approximately 108 μm (at $1/e^2$ intensity) with the estimated 20.7 fs pulse duration and an approximately $1.0 \times 10^{13}$ W/cm² peak intensity. Even though the peak intensity is relatively high for 400 nm pulses, obvious filamentation is not observed in our experiment. Then two 50 μm thick fused silica
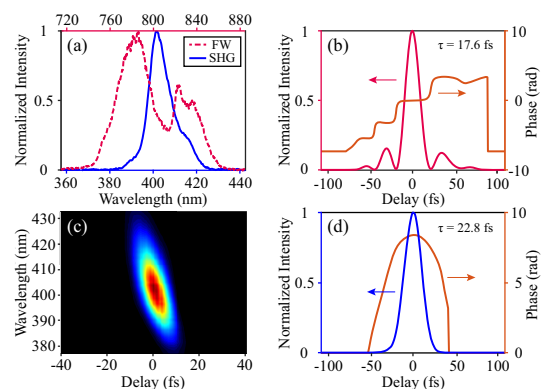


**Fig. 1.** Experimental set-up. Periscope1, composed of two Ag-coated mirrors to change the fundamental wavelength (FW) pulses polarization from p to s. AgM, Ag-coated mirror; Periscope2, composed of a dichroic mirror and a UV-enhanced Al-coated (UV-Al) mirror to achieve the separation of the FW and SHG beams. FM1–FM4, UV-Al concave mirrors (*f* = 0.75, 0.5, 0.75, and 0.5 m, respectively) with an average reflectivity of 92%; AlM, UV-Al mirror; CM1 and CM2, chirped mirrors; FS1 and FS2, 200 μm and 350 μm thick fused silica plates. The inset shows the photograph of near-field spot of the final output beam.



**Fig. 2.** Characterization of the FW and SHG pulses. (a) FW (red) and SHG (blue) spectra. (b) Retrieved pulse envelope (red) and phase (orange) of FW pulses. (c), (d) Measured SD-FROG trace and retrieved pulse envelope (blue) and phase (orange) of SHG pulses.

(FS) plates are placed at the Brewster angle before and after the focal point. Their accurate positions are carefully adjusted to achieve maximal spectral broadening under the prerequisites of maintaining good beam quality and high conversion efficiency. Finally, the distance between the two plates is approximately 7 cm. Unlike a 800 nm MPC, the beam quality is more easily degraded during the spectral broadening process of 400 nm pulses, as exhibited in [24]. The beam quality degradation can be partly interpreted as the formation of multifilamentation caused by the small-scale self-focusing (SSSF), which is the consequence of the amplified spatial perturbation (or noise) of the laser beam. The noise gain is mainly determined by the initial beam noise condition and the nonlinear phase accumulation, which can be characterized by the B integral [25]. The B integral is defined as $B = kLn_2I$, in which, $k = 2\pi/\lambda$, $\lambda$ is the laser wavelength, $L$ and $n_2$ are the thickness and nonlinear refractive index of mediums respectively, and $I$ is the pulse intensity. With shorter wavelength and larger $n_2$ [26], the 400 nm pulses will accumulate a larger B integral during the spectral broadening process, which is more likely to cause a larger noise gain and intensify the SSSF. Therefore a thinner FS plate, i.e., smaller $L$, is chosen to decrease the B integral accumulated in the solid plates. Thus the beam quality degradation caused by SSSF (i.e., multifilamentation) can be effectively avoided. At the same time, the obvious cone-emission and excessively high intensity arising from self-focusing can also be suppressed. The spectrum is broadened to nearly 360–450 nm, supporting a 9 fs FTL pulse duration, and the spectral broadening process is shown in Fig. 3(a). After that, the remaining pulse energy is 17.6 µJ. Considering the reflectivity of FM1, the actual energy loss caused by spectral broadening is 8%, which is close to the 6% of 800 nm pulses [25]. It indicates that the ionization effect in our experiment is effectively suppressed. Simultaneously, the near-field spot profile almost maintains a complete circle without evident rings, which further ensures the high conversion efficiency. Then the beam is collimated by FM2, and with 4 bounces on a pair of CMs (Ultrafast Innovation, CM82), a total −200 fs$^2$ excessive chirp is introduced. The residual negative chirp is compensated by a Brewster angle placed, fixed-thickness FS plate, whose thickness can be chosen in a step of 50 µm for fine dispersion adjustment. SD-FROG is used to diagnose and optimize the pulse compression. By choosing a proper glass thickness, 9.9 fs clean pulses can be obtained, as shown in Fig. 3(b). The pulse energy after compression is 13.7 µJ, which corresponds to a 66% total efficiency of the first stage. The energy decrease is mainly caused by the reflection loss of the focusing mirrors and CMs. The efficiency of the CMs after 4 reflections is approximately 85%, which is lower than the nominal value. We believe that it is caused by surface diffraction and two-photon absorption of the mirrors' coating [27].

In the second stage, FM3 is used to focus the laser beam again. The diameter of the beam waist after focusing is 153 µm (at $1/e^2$ intensity), and the corresponding pulse peak intensity is estimated to be approximately $6.9 \times 10^{12}$ W/cm$^2$. Here, two 50 µm thick FS plates are placed using the same strategy as the first stage, the distance between them is 6 cm. The maximal spectral broadening is obtained when the best pulse compression is achieved at the beam waist position. Finally, the supercontinuum can span 350–500 nm, which supports an FTL pulse duration of sub-5 fs, with less than 8% energy loss. The spectral broadening process is shown in Fig. 3(d). It is worth mentioning that the broadened spectrum shows a significant redshift which
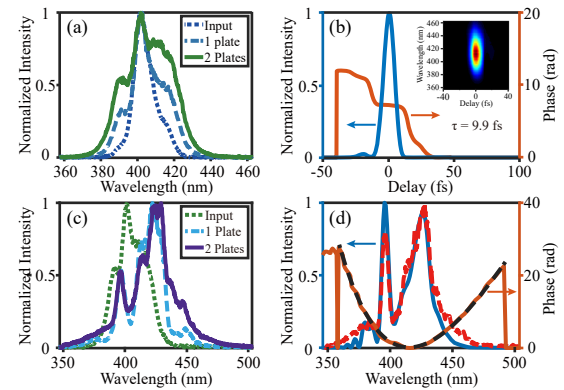


**Fig. 3.** (a), (c) Spectral broadening process of first and second MPC generation stage. (b) Measured trace (inset) and retrieved pulse envelope (blue) and phase (orange) of the compressed pulses of the first stage. (d) Measured spectrum (red), retrieved spectrum (blue), and retrieved phase (orange) of the uncompressed pulses of the second stage. The black dash line is the third-order polynomial fitting of the spectral phase.

is quite distinct from the general spectral blueshift of 800 nm pulses [19,21]. We infer that this phenomenon partly results from the small positive third-order dispersion (TOD) causing a slight steepening of the front of the pulses. This type of pulse envelope develops a redshift of the broadened spectrum.

After collimated by FM4, the diagnostic of uncompressed pulses is performed directly. As shown in Fig. 3(d), a high-quality FROG reconstruction is achieved, which provides the precondition for accurate dispersion analysis. The third-order polynominal fitting (very close to the retrieved phase curve) indicates that the group delay dispersion (GDD; 110 fs$^2$) and TOD (40 fs$^3$) are almost equal to the dispersion introduced by 2.2 m long air. According to the result of dispersion analysis, we use ten reflections of a pair of rectangular CMs (Layertec, −25 fs$^2$/bounce at 340–440 nm, designed for compensating the material dispersion of FS or air, including TOD compensation) to introduce excessive negative GDD and TOD, and then the FS2 is used to compensate the residual negative dispersion. Here, we introduce the Fresnel reflected part (approximately 200 nJ) of the beam into the SD-FROG for pulse characterization. By choosing an appropriate thickness of FS2, an ultrashort pulse duration of 5.2 fs is retrieved, as shown in Fig. 4, with a reconstruction error of 0.0041. As a result of the accurate dispersion compensation, the main pulse contains above 88% of the energy of the whole pulse, which can provide more effective energy for strong-field experiments. However, owing to the energy loss caused by the reflections of the focusing mirrors and the CMs, a pulse energy of 8.6 µJ remains. As shown by the inset photograph in Fig. 1, the near-field spot has a Bessel-like distribution, and the energy of the central bright spot is 7.8 µJ, which accounts for 90% of the total energy. The total conversion efficiency of the second stage is 57%, and the overall conversion efficiency of the two stages is 37.5%. Because the total energy loss of the two stages in the spectral broadening process is lower than 16%, the output efficiency is likely to be greatly improved with specially designed and coated broadband NUV mirrors. The energy stability is measured before dispersion compensation with CMs, as shown in Fig. 5(a), the rms fluctuation over one hour is 0.69% and meanwhile the measured energy stability of
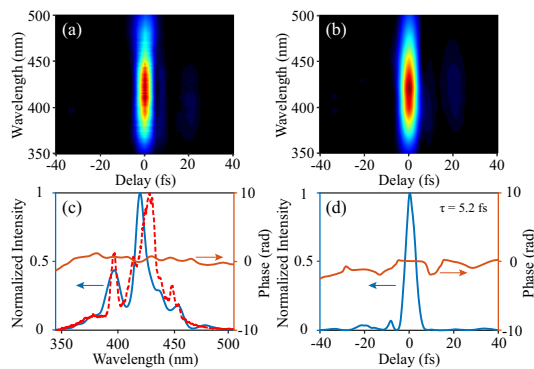
**Fig. 4.** Characterization of the final output few-cycle blue pulses. (a), (b) Measured and reconstructed SD-FROG traces. (c) Measured (red) and retrieved (blue) spectrum, and retrieved phase (orange). (d) Retrieved pulse envelope (blue) and phase (orange).

the FW pulses is 0.36%. This acceptable energy stability degradation is the consequence of energy jitter amplification during the intensity-dependent nonlinear SHG process. By focusing the output beam with a $f = 400$ mm lens, we check the far-field spot, as shown in Fig. 5(b). The excellent beam profile indicates that even though undergoing multiple linear focusing and nonlinear spectral broadening, the beam quality still maintains a high performance.

In conclusion, we have compressed blue pulses to 5.2 fs with high energy stability and excellent beam quality, by directing the relatively broadband and short 400 nm laser pulses into a two-stage MPC apparatus. With such input pulses and two-stage configuration, thinner and fewer plates can be used to achieve spectral broadening. As a result, multifilamentation formation, excessive ionization, and high-order nonlinear dispersion accumulation during the spectral broadening process are effectively avoided. The generated supercontinuum covers the region of approximately 350–500 nm. With fine dispersion control in the whole apparatus, an ultrashort and clean pulse compression, with near to 90% of the energy contained in the main pulse, is achieved. In our experiment, the spectrum-shaped FW pulse is obtained by broadening the chirped pulses in an HCF. However the required spectrum can also be achieved by spectrally shaping the current commercially available multi-mJ level 20–25 fs laser, which can deliver more energy for the SHG process. We believe that it is possible to generate above 100 μJ level ultrashort blue pulses with 3 mJ FW pulses and a more compact MPC apparatus in vacuum conditions [22], when a conservative 10% SHG conversion efficiency is take into consideration. In addition, our scheme is very suitable to compress the SHG pulses of a post-compressed ytterbium-doped ultrafast fiber laser for generation of high-repetition-rate few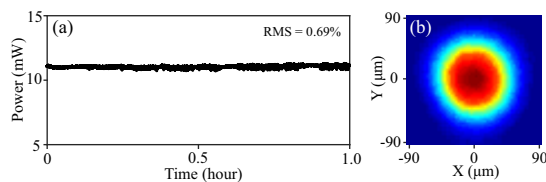-cycle green pulses. On account of the high flexibility, robustness, and low cost, this scheme is very suitable for extensive applications in ultrafast, strong-field studies.

**Disclosures.** The authors declare no conflicts of interest.

**Data availability.** Data underlying the results presented in this Letter are not publicly available at this time but may be obtained from the authors upon reasonable request.

**REFERENCES**

1. J. Li, J. Lu, A. Chew, S. Han, J. Li, Y. Wu, H. Wang, S. Ghimire, and Z. Chang, Nat. Commun. **11**, 2748 (2020).
2. M. Ludwig, G. Aguirregabiria, F. Ritzkowsky, T. Rybka, D. C. Marinica, J. Aizpurua, A. G. Borisov, A. Leitenstorfer, and D. Brida, Nat. Phys. **16**, 341 (2020).
3. D. Pengel, S. Kerbstadt, D. Johannmeyer, L. Englert, T. Bayer, and M. Wollenhaupt, Phys. Rev. Lett. **118**, 053003 (2017).
4. R. Wang, Q. Zhang, C. Ran, W. Cao, and P. Lu, Opt. Lett. **45**, 1383 (2020).
5. A. D. Shiner, C. Trallero-Herrero, N. Kajumba, H. C. Bandulet, D. Comtois, F. Légaré, M. Giguére, J. C. Kieffer, P. B. Corkum, and D. M. Villeneuve, Phys. Rev. Lett. **103**, 073902 (2009).
6. C. Lai, G. Cirmi, E. Granados, S. Huang, P. Keathley, A. Sell, K. Hong, J. Moses, and F. Kärtner, in *2012 Conference on Lasers and Electro-Optics (CLEO)*, (2012), pp. 1–2.
7. S. D. Khan, Y. Cheng, M. Möller, K. Zhao, B. Zhao, M. Chini, G. G. Paulus, and Z. Chang, Appl. Phys. Lett. **99**, 161106 (2011).
8. H. T. Chang, M. Zürch, P. M. Kraus, L. J. Borja, D. M. Neumark, and S. R. Leone, Opt. Lett. **41**, 5365 (2016).
9. J. Liu, Y. Kida, T. Teramoto, and T. Kobayashi, Opt. Express **18**, 4664 (2010).
10. C. Li, X. Zhou, F. Zhai, Z. Li, F. Yao, R. Qiao, K. Chen, M. T. Cole, D. Yu, Z. Sun, K. Liu, and Q. Dai, Adv. Mater. **29**, 1701580 (2017).
11. F. Xiao, X. Fan, L. Wang, D. Zhang, J. Wu, X. Wang, and Z. Zhao, Chin. Phys. Lett. **37**, 114202 (2020).
12. R. B. Varillas, A. Candeo, D. Viola, M. Garavelli, S. De Silvestri, G. Cerullo, and C. Manzoni, Opt. Lett. **39**, 3849 (2014).
13. T. Kanai, X. Zhou, T. Sekikawa, S. Watanabe, and T. Togashi, Opt. Lett. **28**, 1484 (2003).
14. P. Baum, S. Lochbrunner, and E. Riedle, Opt. Lett. **29**, 1686 (2004).
15. E. Keil, P. Malevich, and J. Hauer, Opt. Express **29**, 39042 (2021).
16. O. Dühr, E. T. J. Nibbering, G. Korn, G. Tempea, and F. Krausz, Opt. Lett. **24**, 34 (1999).
17. J. C. Travers, T. F. Grigorova, C. Brahms, and F. Belli, Nat. Photonics **13**, 547 (2019).
18. C. Brahms, F. Belli, and J. C. Travers, Phys. Rev. Res. **2**, 043037 (2020).
19. C.-H. Lu, Y.-J. Tsou, H.-Y. Chen, B.-H. Chen, Y.-C. Cheng, S.-D. Yang, M.-C. Chen, C.-C. Hsu, and A. H. Kung, Optica **1**, 400 (2014).
20. Y.-Y. Liu, K. Zhao, P. He, H.-D. Huang, H. Teng, and Z.-Y. Wei, Chin. Phys. Lett. **34**, 074204 (2017).
21. M. Seo, K. Tsendsuren, S. Mitra, M. Kling, and D. Kim, Opt. Lett. **45**, 367 (2020).
22. M. Stanfield, N. F. Beier, S. Hakimi, H. Allison, D. Farinella, A. E. Hussein, T. Tajima, and F. Dollar, Opt. Express **29**, 9123 (2021).
23. C. H. Lu, T. Witting, A. Husakou, M. J. J. Vrakking, A. H. Kung, and F. J. Furch, Opt. Express **26**, 8941 (2018).
24. M. Canhota, R. Weigand, and H. M. Crespo, Opt. Lett. **44**, 1015 (2019).
25. V. N. Ginzburg, A. A. Kochetkov, S. Y. Mironov, A. K. Potemkin, D. E. Silin, and E. A. Khazanov, Radiophys. Quantum Electron. **62**, 849 (2020).
26. Y. E. Geints, A. M. Kabanov, A. A. Zemlyanov, E. E. Bykova, O. A. Bukin, and S. S. Golik, Appl. Phys. Lett. **99**, 181114 (2011).
27. O. Razskazovskaya, T. T. Luu, M. Trubetskov, E. Goulielmakis, and V. Pervak, Optica **2**, 803 (2015).

**Fig. 5.** (a) Energy stability of the spectrally broadened pulses of the second stage. (b) Measured far-field spot of the final output beam.